*Artificial Intelligence Review* **12:** 245–262, 1998.



# Three-Dimensional Image Reconstruction Procedure for Food Microstructure Evaluation

K. DING[1] and S. GUNASEKARAN[2]
[1]*Universal Instruments Corporation, Binghamton, NY, USA;*
[2]*Biological Systems Engineering, University of Wisconsin-Madison, Madison, WI 53706, USA*

**Abstract.** Confocal laser scanning microscopy (CLSM) is a noninvasive technique for evaluating the microstructure of foods and other materials. CLSM provides several sequential subsurface layers of two-dimensional (2-D) images. An image processing algorithm was developed to reconstruct these 2-D layers into a three-dimensional (3-D) network. Microstructure of fat globules in cheese was used as an example application. The validity of the image reconstruction algorithm was evaluated by processing several layered digital images of known shape and size. Differences between the original and reconstructed images were 2–5% in terms of object size and 1–8% in terms of shape.

**Key words:** Confocal laser scanning microscopy (CLSM), food microstructure, image processing, computer vision, cheese, fat globules

## Introduction

The study of physical and functional properties of foods is hindered by the inherent inhomogeneities of foods. Instrumented measurement of textural properties involves measuring stress, strain, and time effects. The results obtained are in response to forces acting on an underlying organized structure. Perhaps the best approach is to study how sensory and mechanical responses relate to structural organization (Stanley 1987). Observing microstructure and changes in it with perturbations of composition or physical forces can reveal parameters directly related to texture. In fact, it is the microstructure which actually determines the sensory and mechanical characteristics of a food. Foods having similar microstructures can be loosely grouped together as foods that have similar textures (Kalab et al. 1995). Thus, knowledge of microstructure must be antecedent to any plan aimed at either manipulation or regulation of texture.

A variety of microscopic techniques are available to examine food microstructure. These include light microscopy, scanning electron microscopy (SEM), transmission electron microscopy (TEM) and confocal laser

scanning microscopy (CLSM). SEM and TEM offer the advantage of high resolution, but sample preparation procedures are laborious and may lead to artifacts (Kaláb 1984; Liboff 1988). CLSM offers an alternative method to observe food structure without disturbing the internal structure (Brakenhoff et al. 1988; Brooker 1991).

One of the major problems associated with traditional microscopic methods of studying complicated structures is quantification of image features. Computer imaging is an extremely powerful technique for extracting and quantifying features for quality assessment and control. It can also help in understanding mechanisms of complex processes that alter product characteristics. It offers the advantages of accurate quantification of images and rapid data handling. Almost all instruments used to provide an enlarged view of food systems can be used with image analysis, either through direct interfacing to a light or electron microscope or by scanning outputs such as photographs or negatives (Stanley 1987).

Quantitative evaluation of food microstructure is increasing. Ruegg and Moor (1987) determined the size distribution and shape of curd granules in hard and semi-hard Swiss cheeses. The quantification of microstructure is highly facilitated by computer image analysis (Inoue 1986). Within the past few years, computer image processing has become increasingly popular in the food industry (Gunasekaran and Ding 1994; Gunasekaran 1996). Applications range from quality parameters of food grains (Gunasekaran et al. 1987; Gunasekaran et al. 1988) and microscopic characteristics of leaves (Wen and Gunasekaran 1992) to intramuscular fat in muscle (Ishii et al. 1992). Ali and Robinson (1985) used a digitizer tablet to transfer micrograph images for analysis to evaluate size distribution of casein micelle in camel milk. Recently, Holcomb et al. (1992) investigated textural changes in dairy products by image analysis. Ding and Gunasekaran (1992 and 1993) presented preliminary results of microstructure study of cheese and milk gel using computer image processing. An example of the use of digital image analysis to quantify structural features of cheese was given for string cheese (Taneya et al. 1992).

We recently applied confocal microscopy to compare the size and shape of fat globules in reduced-fat Cheddar cheese where the globules were coated either with native milk proteins in a non-specific fashion, lactalbumin (heat-denatured $\beta$-lactoglobulin and $\alpha$-lactoalbumin) or $\beta$-casein (Everett et al. 1995). These results were based on analysis of 2-D layered images. In order to describe the internal structure more completely, a 3-D network would be most suitable. Owing to the development CLSM and the increased computational power and speed of computers, 3-D microscopy is becoming the latest trend in the microstructural analysis of foods (Gunasekaran 1996; Vodovotz

et al. 1996; Blonk and van Aalst 1993). There are some commercial 3-D reconstruction softwares suitable for CLSM images. However, they are either too expensive or too specific for biomedical-type applications.

Our objectives were: 1) to develop a 3-D image reconstruction algorithm from 2-D layered CLSM images and 2) to validate the algorithm by processing several known 3-D elements.

## Confocal Laser Scanning Microscopy

Confocal microscopy is characterized by the ability to make selective observations of one plane within a specimen, unaffected by the image of out-of-focus regions above and below the plane. This technique is known as optical slicing (Rao et al. 1992). In Figure 1, the optical slicing technique used in the CLSM is illustrated schematically. When a conventionally imaged object is displaced from best focus, the image contrast decreases but the spatially averaged intensity remains the same. In a confocal system, however, the image of defocused surface appears darker than if it were in focus. Thus, confocal optics can be said to have axial resolution in addition to lateral resolution. As a consequence, it is possible to extract topographic information from a set of confocal images taken over a range of focal planes. In order to form a confocal image, the signal is recorded as the object is scanned relative to the image of the point source in a plane parallel to the focal plane. Multiple confocal image slices are obtained by repeating the process at various levels of object defocus. By focusing at different heights (along the z-axis) on the object, a 3-D topographical map of the object is obtained. The resolution in the z-direction (axial resolution, $\Delta$z) depends upon the numerical aperture of the lens, the degree to which the pinhole is open, and the wavelength of the laser light. If the confocal pinhole is fully opened, the microscope becomes a conventional scanning light microscope with reduced lateral resolution and larger depth of field in the z-direction. The minimum $\Delta$z is 0.5 $\mu$m (Brakenhoff et al. 1988) which is very difficult to achieve using a regular light microscope. Maximum observation depths of 10 $\mu$m to 100 $\mu$m can be achieved, depending on the opacity and absorption characteristics of the specimen (Heertje et al. 1987; Brakenhoff et al. 1988; Brooker 1991). In addition, specimen observations can be made within a plane both transverse to and along the optical axis, compared to conventional light microscopy where only images transverse to the optical axis can be made (Brakenhoff et al. 1988). Perhaps a disadvantage of the CLSM is that the minimum resolvable area is approximately 0.2 $\mu$m $\times$ 0.2 $\mu$m. For additional description of the CLSM the readers are referred to a recent article by Vodovotz et al. (1996).

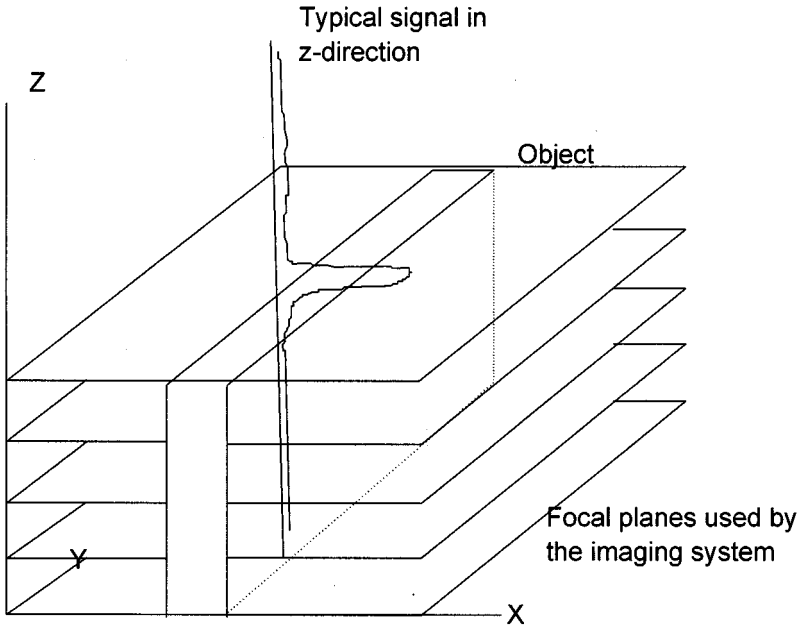


*Figure 1*. Schematic representation of optical slicing in CLSM (based on Rao et al. 1992).

## Image Reconstruction

Since images obtained from a microscope are specific to the settings used, the following was considered in developing the 3-D reconstruction algorithm. Microstructure of fat globules in cheese is used as the example application. However, the procedure described here and the algorithm developed is suitable for evaluating similar images. Confocal images were taken using an MRC-600 confocal microscope (Bio-Rad Microscience, Ltd.) available at the Integrated Microscopy Resource at the University of Wisconsin-Madison. Additional details of the imaging process used (staining, lens etc.) are described in Ding (1994). The resolvable area called "pixel" is an element square of a 2-D image that was approximately 0.3 $\mu$m $\times$ 0.3 $\mu$m. The separation between observation planes was set at 0.5 $\mu$m, which is the smallest separation for the 40$\times$ magnification lens. For each specimen, 81 adjacent planes (layers) were observed. Thus, the observation depth was 40 $\mu$m. The 3-D image was 256 $\times$ 256 pixels and 8-bit gray-scale image (256 levels of gray). CLSM provides a sequence of 2-D layered images. Some 2-D image layers of the cheese are presented in Figure 2. The 3-D image of the fat globules in Cheddar cheese reconstructed per the procedure described herein is shown in Figure 3.

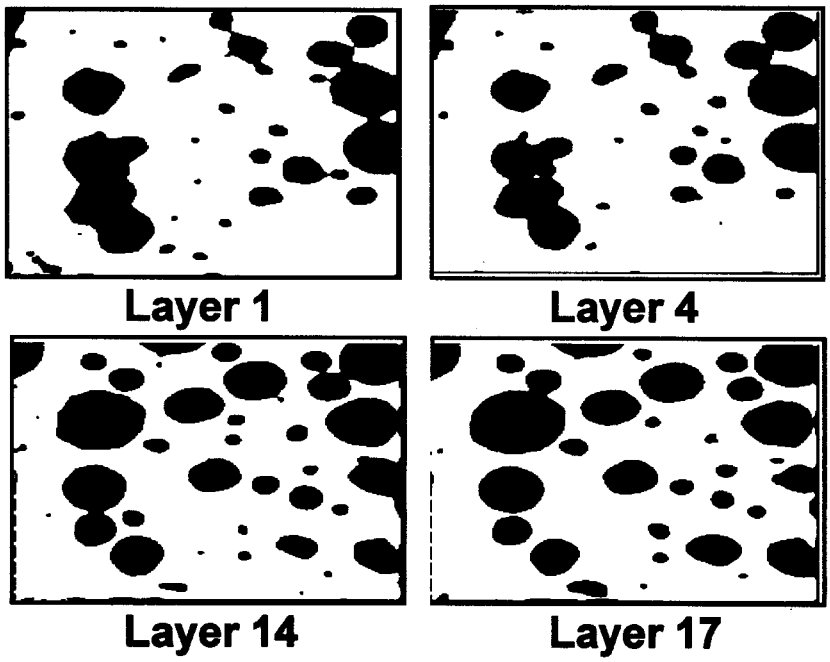


*Figure 2*. Some 2-D images from CLSM showing fat globules in Cheddar cheese (black areas) at different subsurface layers.

Before the layered images were reconstructed, they were subjected to background correction and scaled as explained below. The image analysis software Optimas (Bioscan Corp., Seattle, WA) was used as the base for developing algorithms.

*Background correction*

Because of the lens and lighting problems, 2-D CLSM micrographs often are brighter in the center and fade out gradually towards the edges. An uneven background may make it impossible to set a single gray scale threshold value for image segmentation.

To even out the background, a quadratic polynomial surface was used to fit the background by statistical regression. Then the quadratic polynomial surface was subtracted from the original image surface. The average intensity of the image was added back to this. To simplify the description, a line of a 2-D image is selected as an example, and the background correction procedure is illustrated in Figure 4a. The original line of the image has low intensity in the middle and high intensity on either side. The corrected line of the image has fairly uniform intensity throughout. Figure 4b shows a 2-D layered image of

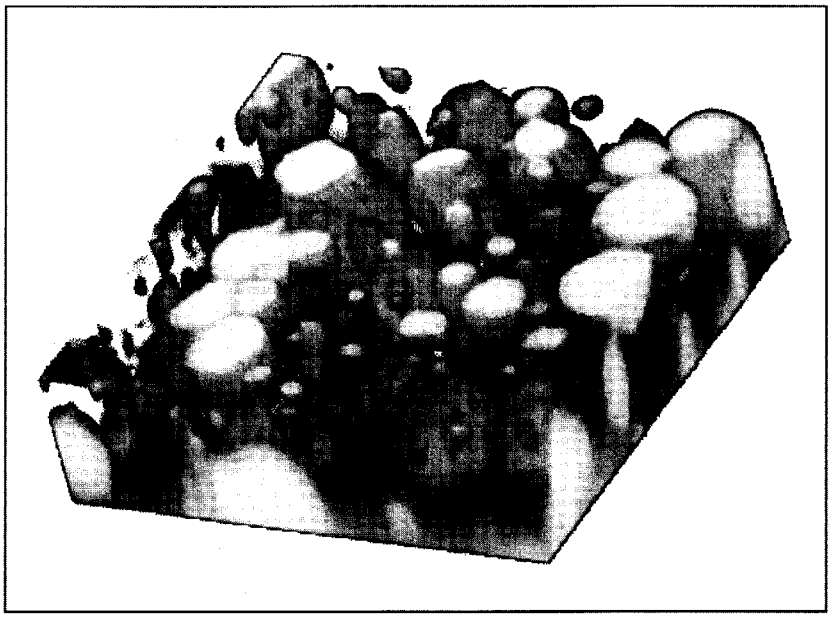

*Figure 3*. A 3-D image of fat globules in Cheddar cheese reconstructed from 2-D image layers from CLSM (the brighter areas represent fat globules chopped during specimen preparation).

the cheese *before* the background correction. (The central part is darker than other parts because this is an intensity reversed image, i.e., black and white are reversed for image processing, of a CLSM micrograph.) Figure 4c shows the same 2-D image layer *after* the background correction. This image has an approximately even background.

The background can only be corrected approximately, however, and some minor information about the image may be lost during the process. Before background correction, some small fat globules at the image boundary are visible. After the background correction, they are invisible. Since the lost information is usually small, the background correction technique has been widely used for microscopic imaging.

*Image segmentation*

Image segmentation is normally achieved by setting a threshold based on image histogram. However, because of the lighting problem, the brightness in different layers of the CLSM slices was different. Thus, even after background correction, although it was possible to use a single threshold for one 2-D layer, it was still impossible to set a fixed threshold for all layers. In addition, because it was very hard to obtain proper bimodal histograms of images from

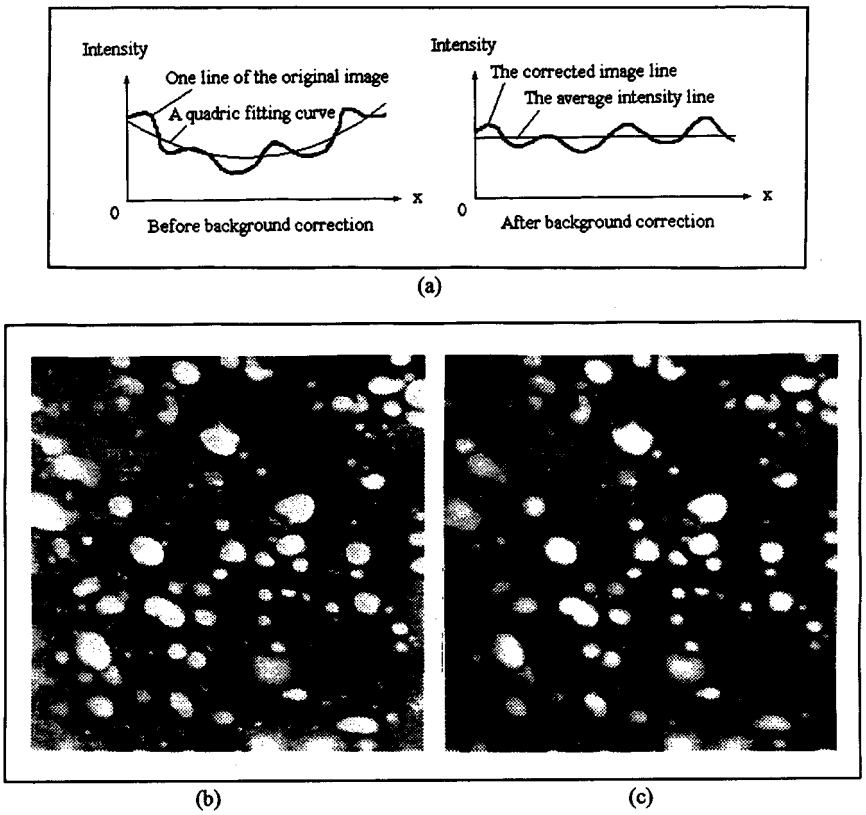


*Figure 4.* Description of background correction procedure (a); and an image before (b) and after (c) background correction.

all layers, the optimal thresholding cannot properly segment fat globules from the background. Since there was no shrinkage during the CLSM sample preparation, the threshold of each 2-D layer could be set according to the overall fat content of cheese assuming that the fat was distributed uniformly. Given the small sample size used, this is a very reasonable assumption. The fat content of the low-fat Cheddar cheese used in this study was 13.9%. Thus, 13.9% of the brighter pixels in each 2-D layer was segmented as fat globules (i.e. set as white pixels). For thresholding and other processing operations we used the Optimas Image Analysis Software (Optimas Corporation, Bothell, WA) as the base program.

*Image scaling*

The width of a 2-D image layer was 77 $\mu$m. There were 256 $\times$ 256 pixels per image, so the size of one pixel is 0.3 $\mu$m $\times$ 0.3 $\mu$m. A 2-D image is processed pixel-by-pixel. A 3-D image is processed voxel-by-voxel. A voxel is an element of a 3-D image that should be a cube (Figure 3) in order to be easily processed. However, the distance between two adjacent layers was 0.5 $\mu$m which did not equal the pixel size (0.3 $\mu$m $\times$ 0.3 $\mu$m) in a 2-D image layer. Therefore, the voxel shape was not cubical. To reconstruct the 3-D image that has cubic-shaped voxels, image scaling was performed using the built-in function of the Optimas software. After scaling all 2-D layered images, they could be put together to construct a 3-D image. Since the 2-D images were digitized, each could be represented as a 2-D matrix. Thus, a 3-D image was a 3-D matrix and all the voxel dimensions were 0.5 $\mu$m $\times$ 0.5 $\mu$m $\times$ 0.5 $\mu$m.

*Object identification*

The image layers were scanned from top to bottom and left to right. The microstructural elements of interest (fat globules) were numbered voxel-by-voxel by a process known as image labeling. The digitized voxel values (intensities) were the elements of the 3-D matrix. Figure 5 illustrates the schematic diagram of a $6\times6\times6$ 3-D matrix. Before scanning, the 3-D image was a binary image (a binarized 3-D matrix).

White voxels were labeled as 0 and black voxels were labeled by a large number *b*. We selected *b* to be larger than the maximum expected number of globules (or objects of interest). We set b = 32768 because it represents half the possible number of pixels (i.e., (256 $\times$ 256)/2).

During scanning, the boundary voxel values were checked in order to distinguish the boundary-chopped and non-chopped fat globules, and the rest of the 3-D image was scanned. For the entire 3-D image, the scanning was actually from the second top layer to the second bottom layer (from layer 1 to layer 4 in Figure 5). For each layer, the scanning was from the second front row to the second back row (from row 1 to row 4 in Figure 5); for each row, the scanning was from second left voxel to the second right voxel (from column 1 to column 4 in Figure 6). To label the boundary-chopped fat globules and boundary non-chopped fat globules separately, two stacks of numbers were selected. Stack C (1 to 1000 with 1 on the top of the stack) was for the boundary-chopped fat globules (reflects our assumption that there were fewer than 1000 boundary-chopped fat globules in the specimen being examined). Stack N (1001 to 32,767 with 1001 on the top of the stack) was

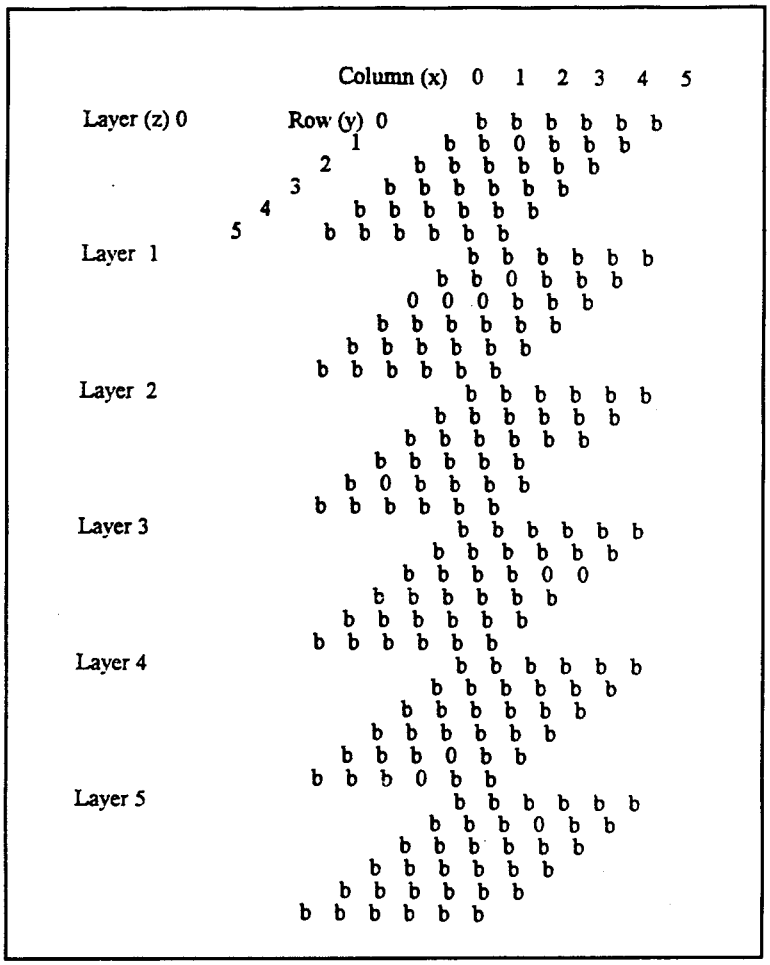


*Figure 5.* Schematic diagram of a 3-D matrix of an image before numbering.

for the boundary non-chopped fat globules. During scanning, the algorithm was as follows.

(1) For each line scanned, only the white voxels (elements of 0 in Figure 5) were processed as they belong to fat globules (or the object of interest) in the 3-D image. It saved much processing time, especially for very low-fat cheeses.

(2) For each white voxel (voxel value = 0), the voxel values of the top, front and left adjacent voxels were checked. If the smallest voxel value of the three adjacent voxels was zero, that voxel may be part of a fat globule that

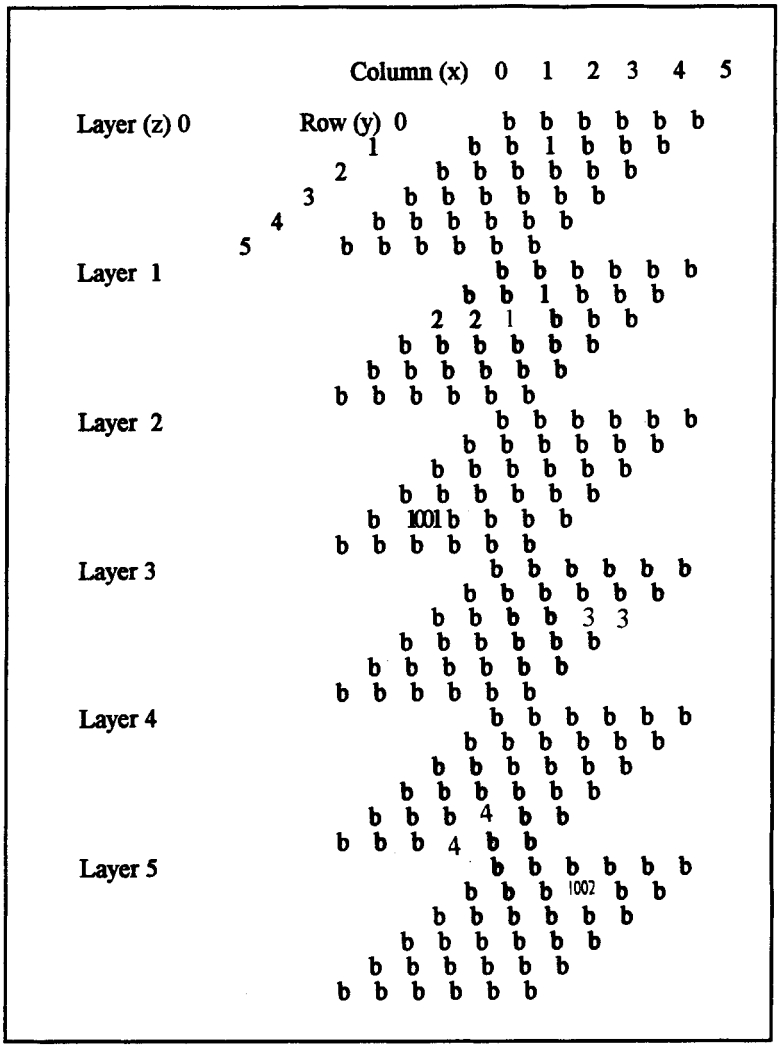


*Figure 6.* Schematic diagram of a 3-D matrix of an image during numbering.

has not been labeled. The algorithm first checks whether the fat globule was chopped by the boundary of the 3-D image as follows.

If one of the three adjacent voxels was a boundary white voxel, that indicates that at least one voxel of the fat globule was on the boundary of the 3-D image. So that fat globule was recognized as a boundary-chopped fat globule. One number on the top of stack C was used. The voxel and the boundary voxel were labeled by that number. For example, the voxel

[x = 2, y = 1, z = 1] should be set to 1 because the top adjacent voxel [x = 2, y = 1, z = 0] was a boundary white voxel. The voxel [x = 1, y = 2, z = 1] should be set to 2 because the adjacent voxel on the left [x = 0, y = 2, z = 1] was a boundary white voxel. Otherwise, the fat globule was not boundary-chopped. One number on the top of stack N was used, and the voxel was labeled by that number. For example, the voxel [x = 1, y = 4, z = 2] should be set to 1001 (the first boundary non-chopped fat globule).

(3) If the smallest value of the three adjacent voxels was greater than zero, that indicates that the fat globule had been labeled and the voxel belonged to the labeled fat globule. Therefore, the voxel was labeled by the smallest number. For example, in Figure 5 the voxel [x = 2, y = 2, z = 1] should be set to 1 because the smallest value of the adjacent voxel [x = 2, y = 1, z = 1] was 1.

(4) If the second or third smallest number was less than the background voxel number ($<$32,767 in our program), that indicates that the fat globule had been labeled by two or more numbers in the upper layers or front lines. In Figure 6, the fat globule of voxels [x = 2, y = 1, z = 1], [x = 2, y = 2, z = 1] and [x = 1, y = 2, z = 1] were labeled by two numbers (1 and 2). Whenever this case occurred, the algorithm would track back and relabel all the voxels to be the same number.

Smaller numbers were always used for relabelling. The second or third smallest number was returned to stack C or stack N, depending on where the number was from. In the case immediately above, the voxels of the fat globule would be relabelled 1; number 2 would be returned back to stack C. So, under normal processing, the voxels labeled 3 and 4 in Figure 6, would have been labeled 2 and 3, respectively. Returning the numbers and reusing them off the top of the stack helped to save computer memory. If all the fat globules in a 3-D image can be labeled by 255 numbers, the data type byte (8 bits) can be used instead of an integer (32 bits) to save memory. A listing of the computer program implementing this algorithm is in Ding (1995).

## Algorithm Validation

Since the exact size and shape of the fat globules in the cheese is not known we have to select a known standard for validating our algorithm. Therefore, following objects were constructed in 23 layers of 2-D digital images (2-D matrixes, Figure 7). The objects were: two spheres (diameter d = 5 $\mu$m and 10 $\mu$m, respectively); one vertical cylinder (diameter d = 5 $\mu$m, height h = 5.5 $\mu$m); one horizontal cylinder (diameter d = 5 $\mu$m, height h = 6.0 $\mu$m); one cylinder (diameter d = 5 $\mu$m, height h = 5.0 $\mu$m) slanted 59 to horizontal plane; and one vertical cylinder (diameter d = 10 $\mu$m, height h = 10 $\mu$m) with

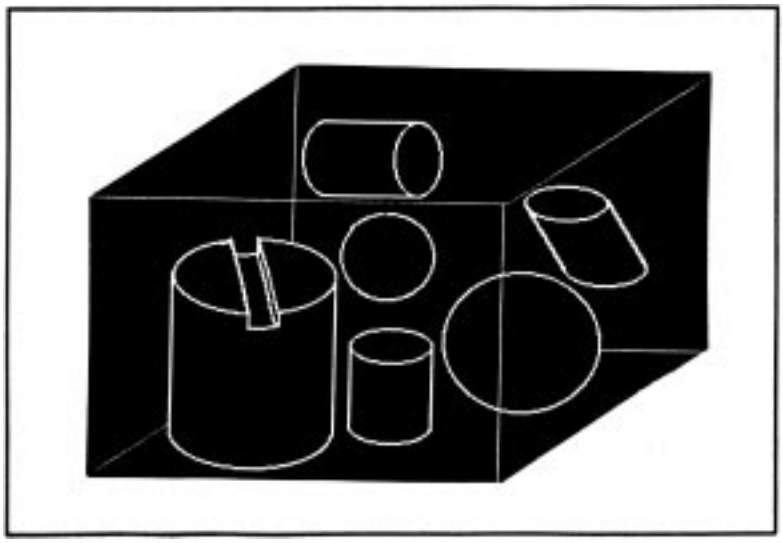

*Figure 7.* Schematic of different objects constructed for algorithm validation.

a notch (width w = 3 $\mu$m, length l = 10 $\mu$m, height h = 1.5 $\mu$m) on the top. The procedure used to construct these images is as follows.

*2-D layered image construction*

A 2-D layered image is a 2-D matrix of pixels. The objects were assigned a pixel value of 255 (white) and the background 0 (black). Since pixel size and distance between adjacent layers of the CLSM layered images in our experiments were known (pixel size = 0.3 $\mu$m $\times$ 0.3 $\mu$m, distance between adjacent layers = 0.5 $\mu$m), the 2-D layered validation images were constructed exactly the same as the 2-D layered CLSM images. The coordinate system used is shown in Figure 8 where each pixel location in the image of layer i was determined by:

$$X_i = \text{Row number} * \text{Pixel width (0.3 } \mu\text{m)};$$
$$Y_i = \text{Column number} * \text{Pixel length (0.3 } \mu\text{m)};$$
$$Z_i = \text{Layer number} * \text{Distance between two layers (0.5 } \mu\text{m)}.$$

To construct a sphere, the process was initiated at the center of the sphere $[X_c, Y_c, Z_c]$ (Figure 8). The distance between each pixel location $[X_i, Y_i, Z_i]$ and the center of the sphere $[X_c, Y_c, Z_c]$ was calculated. If the distance was greater than the sphere radius R, the pixel was assigned 0 (black). Otherwise the pixel was assigned 255 (white).

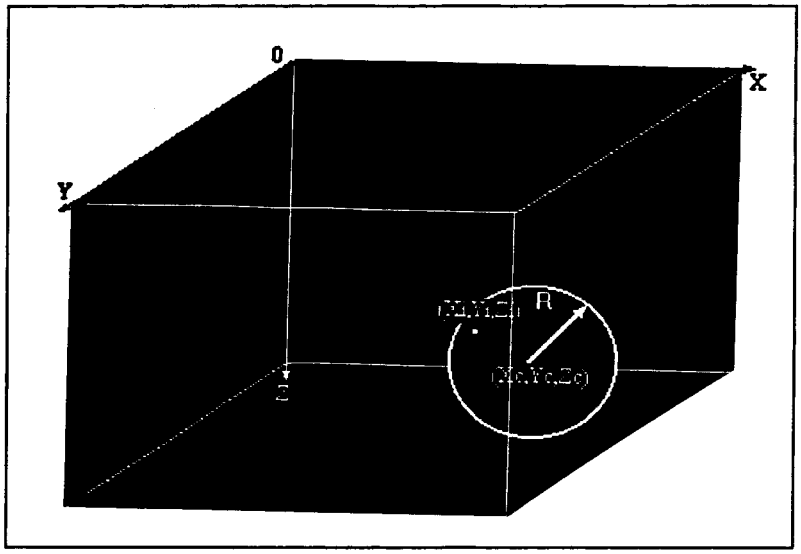


*Figure 8.* Details of construction of a sphere.

To construct a cylinder, the top surface and axis of the cylinder were the starting points (Figure 9). The distance between each pixel $[X_i, Y_i, Z_i]$, and the axis of the cylinder was calculated. In addition, the distance between each pixel $[X_i, Y_i, Z_i]$ to the top surface was calculated. If the distance indicated that the pixel is outside of the cylinder, the pixel was assigned 0; otherwise it is assigned 255. Similarly, after the axis and the width of the notch were known, the pixel $[X_i, Y_i, Z_i]$ was easily found in the cylinder with or without a notch. Similarly, all the objects shown in Figure 7 were constructed in 2-D layers. These 2-D layered images were reconstructed using the algorithm developed. To verify the closeness of the original and reconstructed images, the ideal size and number of surface voxels obtained by geometrical models were compared with the calculated size (diameter) and surface voxel number of the reconstructed image obtained by the 3-D image processing algorithm. For a given geometric shape the number of surface voxels can be calculated (Figure 10) and thus can be used for validating the object shape. The results are shown in Table 1. The relative difference of sphere diameter is about 2–4%, and the relative difference of surface voxel number is about 1–8%. The relative difference was defined as:

$$\textit{Relative difference} = \frac{|\textit{Actual value} - \textit{Reconstructed value}|}{\textit{Actual value}}$$

All objects in the reconstructed 3-D image were successfully separated by the 3-D image processing algorithm and numbered differently. The boundary-

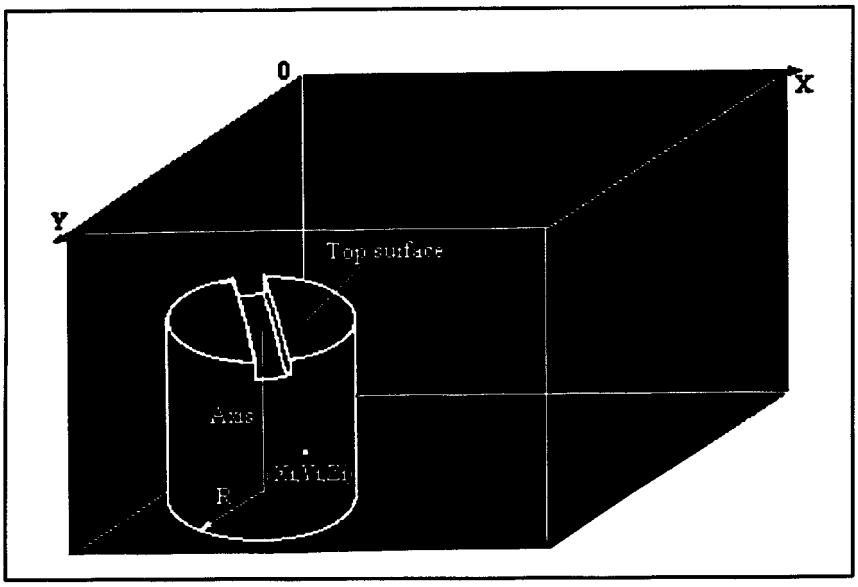


(a) Overall shape of a cylinder with a notch.

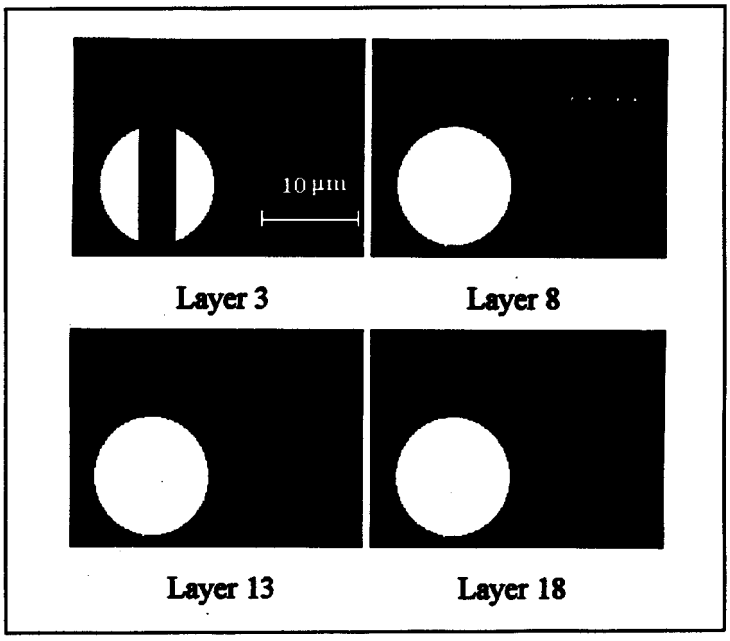


(b) Binary images of four 2-D layers of the above.

*Figure 9.* Details of construction of a cylinder with a notch.

*Table 1.* Validation of 3-D image reconstruction algorithm by comparing size and number of surface voxels of several objects of known size and shape

| Object | Diameter ($\mu$m) | | Relative difference[1] | No. of surface voxels | | Relative d ifference[1] |
|---|---|---|---|---|---|---|
| | Actual | Reconstructed | | Actual | Reconstructed | |
| Sphere | 5.0 | 5.2 | 0.04 | 256 | 236 | 0.08 |
| Sphere | 10.0 | 10.2 | 0.02 | 1028 | 1011 | 0.02 |
| Vertical cylinder | 5.9 | 6.1 | 0.03 | 412 | 404 | 0.02 |
| Horizontal cylinder | 6.2 | 6.5 | 0.04 | 468 | 494 | 0.06 |
| Inclined cylinder | 5.7 | 5.9 | 0.02 | 382 | 380 | 0.01 |
| Cylinder with notch | 11.4 | 11.3 | 0.02 | 1718 | 1621 | 0.06 |

[1] Relative difference = (Actual − Reconstructed)/Actual.

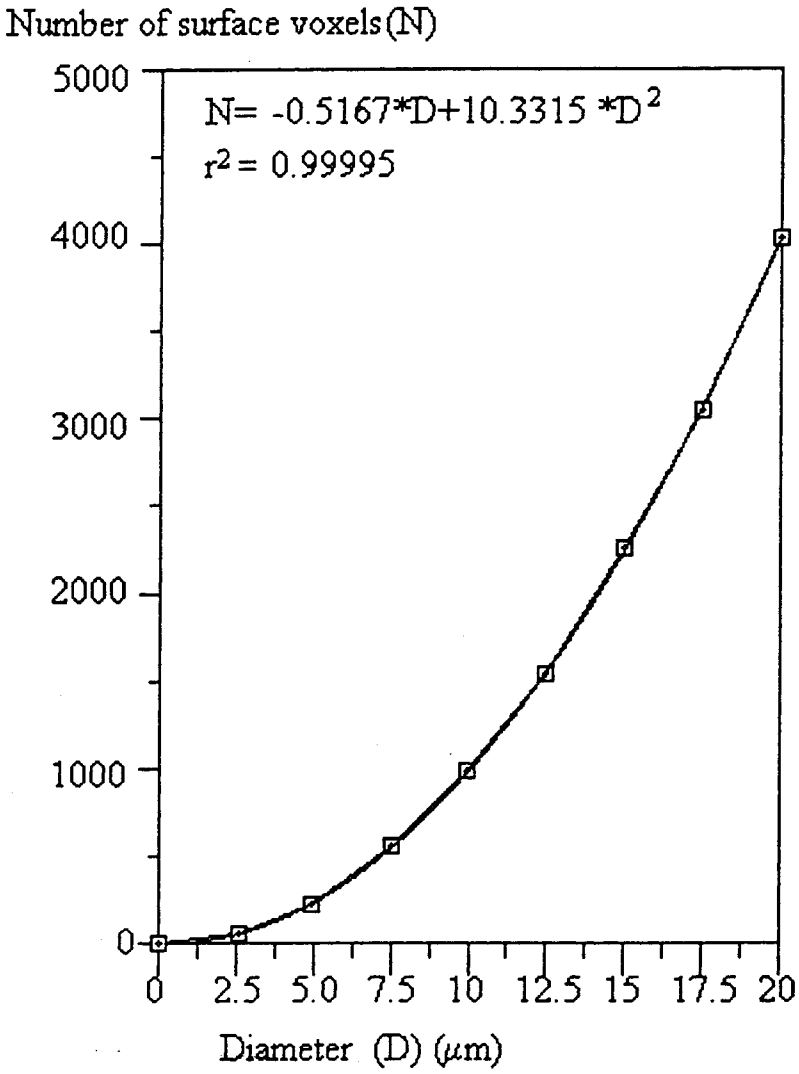


*Figure 10.* Number of surface voxels vs. diamter of a sphere.

touching object, the larger sphere, was also recognized by the 3-D image processing algorithm correctly. The concave-shaped object, the cylinder with notch, was initially numbered as two objects in the top layers. The 3-D image processing algorithm successfully recognized them to be parts of the same object when it processed the bottom layer of the notch and backtracked correctly.

## Conclusions

An image-processing algorithm was developed to reconstruct several sequential 2-D image layers obtained from a CLSM into a 3-D image. An example application of reconstructing fat globules in cheese was considered. The algorithm was evaluated for its validity by reconstructing several 2-D layered digital images of objects of known size and shape. The algorithm performed very satisfactorily. Differences between the original and reconstructed images were 2–5% in terms of object size and 1–8% in terms of shape.

## References


Ali, M. Z. & Robinson, R. K. (1988). Size Distribution of Casein Micelles in Camel's Milk. *J. Dairy Res.* **52**: 303–307.

Blonk, J. C. G. & van Aalst, H. (1993). Confocal Scanning Light Microscopy in Food Research. *Food Res. Int.* **26**(4): 297–311.

Brakenhoff, G. J., van der Voort, J. T. M., van Spronsen, E. A. & Nanninga, N. (1988). 3-Dimensional Imaging of Biological Structures by High Resolution Confocal Scanning Laser Microscopy. *Scanning Microscopy* **2**(1): 33–40.

Brooker, B. E. (1991). The Study of Food Systems Using Confocal Laser Scanning Microscopy. *Microscopy and Analysis* (Nov.): 13–15.

Ding, K. & Gunasekaran, S. (1992). Image Processing for Cheese Microstructure Characterization. *Presented at Food Structure 1992 Meeting of Scanning Electron Microscopy International*. Chicago, IL.

Ding, K. & Gunasekaran, S. (1993). Milk Gel and Microstructure Classification Using Machine Vision. *Presented at 1993 IFT Meeting*. Chicago, IL.

Ding, K. (1995). *Food Shape and Microstructure Evaluation with Computer Vision*. Unpublished Ph.D. Thesis, University of Wisconsin-Madison, Madison, WI.

Everett, D., Ding, K., Olson, N. & Gunasekaran, S. (1995). Applications of Confocal Microscopy to Fat Globule Structure in Cheese. In Malin, E. L. & Tunick, M. H. (eds.) *Chemistry of Structure/Function Relationships in Cheese*, 321–330. Plenum Publishing Corp.: New York, NY.

Gunasekaran, S., Cooper, T. M., Berlage, A. G. & Krishnan, P. (1987). Image Processing for Stress Cracks in Corn Kernels. *Trans. of the ASAE* **30**(1): 266–271.

Gunasekaran, S., Cooper, T. M. & Berlage, A. G. (1988). Evaluating Quality Factors of Corn and Soybean Using a Computer Vision system. *Trans. of the ASAE* **31**(4): 1264–1271.

Gunasekaran, S. & Ding, K. (1994). Using Computer Vision for Food Quality Evaluation. *Food Technol.* **48**(6): 151–154.

Gunasekaran, S. (1996). Computer Vision Technique for Food Quality Assurance. *Trends in FoodSci. and Tech.* **7**(8): 245–256.

Heertje, I., van der Vlist, P., Blonk, J. C. G., Hendrickx, H. A. C. M. & Brakenhoff, G. J. (1987). Confocal Scanning Laser Microscopy in Food Research: Some Observations. *Food Microstructure* **6**(2): 115–120.

Holcomb, D. N., Pechak, D. G., Chakrabarti, S. & Opsahl, A. (1992). Visualizing Textural Changes in Dairy Products by Image Analysis. *Food Technology* **44**(1): 122.

Inoue, S. (1986). *Video Microscopy*. Plenum Press: New York, NY.

Inoue, S. (1995). Foundations of Confocal Scanned Imaging in Light Microscopy. In J. B. Pawley (ed.) *Handbook of Biological Confocal Microscopy*, 1–14. Plenum: New York.

Ishii, T., Cassens, R. G., Scheller, K. K., Arp, S. C. & Schaefer, D. M. (1992). Image Analysis to Determine Intramuscular Fat in Muscle. *Food Structure* **11**: 55–60.

Kalab, M. (1984). Artifacts in Conventional Scanning Electron Microscopy of Some Milk Products. *Food Microstructure* **3**(2): 95–111.

Kalab, M., Allan-Wojtas, P. & Miller, S. S. (1995). Microscopy and Other Imaging Technique in Food Structure Analysis. *Trends in Food Sci. and Tech.* **6**(6): 177–186.

Liboff, M., Goff, H. D., Haque, Z., Jordan, W. K. & Kinsella, J. E. (1988). Changes in the Ultrastructure of Emulsions as a Result of Electron Microscopy Preparation Procedures. *Food Microstructure* **7**(1): 67–74.

Rao, A. R., Ramesh, N., Wu, F. Y., Mandville, J. R. & Kerstens, P. J. M. (1992). Algorithms for a Fast Confocal Optical Inspection System. *Proceedings of the IEEE Workshop on Applications of Computer Vision*, 298–305.

Rosenberg, M., McCarthy, M. J. & Kauten, R. (1991). Magnetic Resonance Imaging of Cheese Structure. *Food Structure* **10**: 185–192.

Ruegg, M. & Moor, V. (1987). The Size Distribution and Shape of Curd Granules in Traditional Swiss Hard and Semi-Hard Cheeses. *Food Microstructure* **6**: 35–46.

Stanley, D. W. (1987). Food Texture and Microstructure. In H. R. Moskowitz (ed.) *Food Texture*. Marcel Dekker, Inc.: New York, NY.

Taneya, S., Izutsu, T., Kimura, T. & Shioya, T. (1992). Structure and Rheology of String Cheese. *Food Structure* **11**: 61–71.

Velinov, P. D., Cassens, R. G., Greaser, M. L. & Fritz, J. D. (1990). Confocal Scanning Optical Microscopy of Meat Products. *J. of Food Sci.* **55**(6): 1751–1752.

Vodovotz, Y., Vittadini, E., Coupland, J., McClements, D. J. & Chinachoti, P. (1996). Bridging the Gap: Use of Confocal Microscopy in Food Research. *Food Technology* **50**(6): 74–82.

Wen, Y. & Gunasekaran, S. (1992). *Measuring Stomatal Characteristics of Elm Leaves by Machine Vision System*. ASAE Paper No. 927022. ASAE Int. Summer Meeting, Charlotte, NC.

Whallon, J. H., Preller, A. & Wilson, J. E. (1994). Reflection Confocal Imaging of Type I and type III Isozymes of Hexokinase in PC12 Cells. *Scanning* **16**(2): 111–117.